ORIGINAL RESEARCH

Chiral Active β-Glucan Nanoparticles for Synergistic Delivery of Doxorubicin and Immune Potentiation

Jintao Huang[1,*]
Chaoxi Wu[2,*]
Shunqing Tang[3]
Pengjun Zhou[2]
Jianping Deng[1]
Zhen Zhang[1]
Yifei Wang[2]
Zhiping Wang [1]

[1]Guangdong Provincial Engineering Center of Topical Precise Drug Delivery System, School of Pharmacy, Guangdong Pharmaceutical University, Guangzhou 510632, People's Republic of China; [2]Guangzhou Jinan Biomedicine Research and Development Center, Institute of Biomedicine, College of Life Science and Technology, Jinan University, Guangzhou 510632, People's Republic of China; [3]Biomedical Engineering Institute, Jinan University, Guangzhou 510632, People's Republic of China

*These authors contributed equally to this work

Correspondence: Yifei Wang; Zhiping Wang
Email twang-yf@163.com; wzping-jshb@gdpu.edu.cn

Background: β-glucans are chiral polysaccharides with well-defined immunological properties and supramolecular wrapping ability of its chiral feature. However, the exploitation of chiral properties of these nanoparticles in drug delivery systems was seldom conducted.

Methods: β-glucan molecules with different chain lengths were extracted from yeast *Saccharomyces cerevisiae* and thereafter modified. In a conformation transition process, these β-glucan molecules were then self-assembled with anti-cancer drug doxorubicin into nanoparticles to construct drug delivery systems. The chiral interactions between the drug and carriers were revealed by circular dichroism spectra, ultraviolet and visible spectrum, fourier transform infrared spectroscopy, dynamic light scattering and transmission electron microscope. The immune-potentiation properties of modified β-glucan nanoparticles were evaluated by analysis of the mRNA expression in RAW264.7 cell model. Further, the antitumor efficacy of the nanoparticles against the human breast cancer were studied in MCF-7 cell model by cellular uptake and cytotoxicity experiments.

Results: β-glucan nanoparticles can activate macrophages to produce immune enhancing cytokines (IL-1β, IL-6, TNF-α, IFN-γ). A special chirality of the carriers in diameter of 50~160 nm can also associate with higher drug loading ability of 13.9% ~38.2% and pH-sensitive release with a change of pH from 7.4 to 5.0. Cellular uptake and cytotoxicity experiments also prove that the chiral-active β-glucan nanoparticles can be used in anti-cancer nanomedicine.

Conclusion: This work demonstrates that β-glucans nanoparticles with special chiral feature which leading to strong immunopotentiation ability and high drug loading efficiency can be developed as a novel type of nanomedicine for anti-cancer treatment.

Keywords: β-glucan, chiral, nanoparticles, doxorubicin, anti-cancer, drug delivery systems, immune-potentiation

Introduction

Nanotechnology-based materials, nanoparticles in particular, have gained significant attention in biomedical fields with their substantial advantages in both efficacy and safety over conventional pharmaceutical agents.[1–3] Through manipulating molecules and atoms at the nanoscale, one can fabricate functional nanoparticles that can be used in therapeutic and diagnostic modalities.[4–8] For instance, nanoparticles can be formulated with inorganic metallic substance such as gold (Au),[9] silver (Ag),[10] iron (Fe),[11] copper (Cu),[12] titanium (Ti)[13] and zinc oxide (ZnO),[14] employed commonly in the detection, diagnosis, and therapy of several diseases

such as protozoal, bacterial and fungal infections.[15–22] Furthermore, The development of biomacromolecule-based drug delivery carriers, such as albumin, peptides and polysaccharides, for effective delivery of therapeutic compounds or imaging agents, is crucial in the battle against various diseases.[23–27] As their inherent biochemical and biophysical properties including renewability, nontoxicity, biocompatibility, biodegradability and potential biological ability, the exploration of biomacromolecule nanoparticle is now considered to be an essential respect in the drug and medicine field.[28–31]

Helix-forming β-glucans, such as curdlan (CUR), yeast β-glucan (YSG), lentinan (LTN), schizophyllan (SPG) and their derivatives have been extensively exploited in the recent two decades as chiral "hosts" to encapsulate/wrap a wide range of "guests" to form drug/DNA/RNA delivery systems, optical/electrical nanodevices, or organic template to organize gold/silver/carbon nanostructures.[32–35] The development of β-glucan drug carriers has garnered an increasing attention owing to its special chiral interaction with bioactive molecules.[36–38] The supramolecular interactions between β-glucans and pharmaceutical molecules can be based on chiral interactions, instead of using excessive electrostatic/hydrophobic interactions, which are frequently adopted by conventional polymer drug delivery systems that may cause denaturing of tissue proteins and bring damage to the cell membrane.[39] In addition, β-glucan itself has a well-established immunopotentiation ability with low toxicity, demonstrated in clinical trials (YSG).[40] Such adjuvant property may become a "plus" when β-glucan is developed as an anti-cancer drug delivery material. More importantly, the helical motif in β-glucan carriers can also function as a chiral "tag" to track the drug encapsulation or release with the aid of circular dichroism spectroscopy. Therefore, β-glucan is worthy of investigation as an anti-cancer drug carrier based on its unique chirality, immunological property, and self-assembling ability.

In previous studies, β-glucan materials were evaluated as carriers for anti-cancer drugs, especially for the model drug doxorubicin (DOX). However, these studies only regard β-glucan as a plain polysaccharide to carry DOX by non-specific absorption; the helical properties of β-glucan were largely neglected. For example, decellularized yeast cells consisting of β-glucan were directly used as DOX carriers,[41] despite the size of the yeast shell being measured in micrometers, making it too large as an ideal DOX carrier. Zhou and his coworkers developed hydrophobically modified CUR

nanoparticles to load DOX; however, the chirality and bioactivity of β-glucan may be lost due to the extensive chemical modification.[42] Meng and his coworkers developed unique self-assembling dendritic nanostructures based on fungal β-glucan as DOX carrier.[43] However, the relationship between chirality and DOX encapsulation is unclear. Thus, a simpler and more efficient self-assembly approach is needed to explore the chirality and helix-forming nature of β-glucan as an advanced DOX carrier.

The aggregation behavior of β-glucans in solution varies greatly depending on their chain structures, which are also associated with their biological origin. Bacterial β-glucans, such as CUR, have limited solubility in water and tend to form large aggregates driven by hydrophobic interaction.[44] On the other hand, fungal β-glucans (LTN/SPG) are fairly soluble in water and tend to exist in the form of well-dispersed triple helices.[45] In comparison, the solubility of YSG lies between CUR and LTN, and it tends to take the form of micro-nano particles due to the presence of long hydrophilic branches on the main chain.[46] In our previous study, we successfully prepared a series of depolymerized or esterified YSG, but their chiral properties and drug carrying abilities have not been investigated.[47] We also investigated the self-assembly of CUR in DMSO/water system that led to a formation of nanofibers.[48] In this study, we continue to investigate the denaturing/renaturing of YSG in the presence of DOX in an attempt to construct novel chiral nanocarriers (NCs). The major hypothesis is that the unique chirality of β-glucan can be exploited by self-assembly to encapsulate and deliver DOX with an adjuvant immunopotentiation effect. Four different self-assembling YSG-derived nanostructures were evaluated and coded as YG, GG, SSG, and BG. YG, in particular, is obtained by DMSO-mediated renaturing of YSG. GG is obtained by pH-induced renaturing of YSG. SSG is developed from pH-induced renaturing of depolymerized YSG while BG is from DMSO-mediated renaturing of hydrophobically modified YSG (butyrylated YSG). The denaturing/renaturing of these β-glucan compounds was in the presence of DOX to trigger the formation of drug delivery systems. Moreover, their nanostructure, chiral fingerprints, and drug-loading properties were extensively characterized using UV-Vis, CD, FT-IR, TEM, DLS analysis. The immunological properties of the drug carriers were tested by expression of cytokines from a RAW264.7 cell model while in vitro their delivery properties were investigated using a human breast adenocarcinoma cancer cell model.

Materials and Methods
Reagents and Cells

YSG from Baker's yeast was purchased from Tiantian Bioengineering & Technology Co., Ltd (China). Doxorubicin (DOX) were purchased from Macklin (Shanghai, China). Depolymerized YSG and Butyrylated YSG were prepared according to our previous work.[47] Dulbecco's modified eagle medium (DMEM, glutamine, high glucose), penicillin, streptomycin and fetal bovine serum (FBS) were purchased from HyClone (USA). 4′,6-diamidino-2-phenylindole (DAPI) was purchased from Sigma-Aldrich Co. (St. Louis., MO, USA). Dialysis tube (MW cutoff, 1.4 kDa) was purchased from Spectrum Labs (Seoul, Korea). Other reagents used in this work were purchased from Aldrich unless otherwise specified. The human breast cancer cell line (MCF-7) and the mice monocytes-macrophages cell (RAW264.7) both were purchased from the Type Culture Collection of the Chinese Academy of Sciences (Shanghai, China).

Preparation of YG-DOX, GG-DOX, SSG-DOX, BG-DOX NCs

NCs-DOX was prepared in two different self-assembly methods: DMSO-mediated self-assembly and pH-induced self-assembly. For the YG-DOX and BG-DOX, the powder of YSG and BG were dissolved, respectively, in DMSO (10 mg/mL, 1 mL) for over 2 hours in the presence of DOX (1 mg/mL, 1 mL). Then 9 mL deionized water was added into the solution, followed by dialysis against plenty of water for two days to remove the free DOX. For GG-DOX and SSG-DOX, powder of YSG and SSG were suspended in deionized water (1 mg/mL, 9 mL) respectively. To the suspension, NaOH solution was added to adjust the pH to 13.0. Then, 1.0 mL of DOX water solution (DOX: 1.0 mg/mL) was added and the resulting mixture was stirred for 5 min. Next, HCl solution was added into the mixture solution to adjust the pH to 7.4. Similarly, after dialysis in plenty of water over two days to remove the free DOX.

Reverse-Transcription-PCR (RT-PCR)

Total RNA was extracted from RAW264.7 cells using TRIzol reagent (Invitrogen Corp., USA), according to the manufacturer's instructions. cDNAs were synthesized from 1 μg of total RNA from each sample using a high-capacity cDNA reverse transcription kit (Applied Biosystems, USA) and were amplified with mouse-specific primers for IL-1β, IL-6, TNF-α, IFN-γ.

Drug Loading Capacity and Drug Release in vitro

The drug loading capacity (DLC) was defined as the weight percentage of DOX in the NCs and drug encapsulation efficiency (DEE) was defined as the weight percentage of loaded-DOX in the NCs and the given DOX. Firstly, DOX solutions of various concentrations were prepared, and the absorbance at 481 nm was measured to generate a calibration curve for the DLC and DEE calculations from various NCs.[49] Secondly, in order to determine the DLC and DEE, 2.0 mg of lyophilized complex was dispersed in 1 mL of deionized water at room temperature, followed by dilution with 9 mL of DMSO to completely expose the encapsulated DOX. The obtained solution was examined by UV–vis spectroscopy at a wavelength of 481 nm. DEE (%) were calculated according to the following equations:

$$DEE(\%) = \frac{\text{the weight of drug loaded into nanogel}}{\text{the weight of initial drug}} \times 100\% \tag{1}$$

The in vitro pH-triggered sustained release behaviors of NCs-DOX were performed at 37 °C in phosphate buffer saline (pH=7.4) and acetate buffer (pH=5.0). The NCs-DOX (0.5 mg) were dissolved in 1 mL phosphate buffered saline solution (PBS) and were placed in dialysis bags (MWCO 8000 −12,000) and dialyzed against 19 mL of release medium under gentle shaking. At the expected time, 5 mL of the medium was removed and replenished with an equal volume of corresponding fresh release medium. The released DOX was determined by UV–vis measurement at a wavelength of 481 nm to calculate the accumulative DOX release profile, and the percentage release of the drug was plotted against time. All the drug loading and release experiments were performed in triplicate to determine means and SD.

Ultraviolet and Visible Spectrum (UV/Vis)

Absorption spectra from the NCs-DOX solution were taken with a double-beam UV−vis spectrometer (Shimadzu UV-2101PC) in a 0.1 mm/0.2 mm demountable quartz cell (Hellmar GmbH, Germany) with the range of 450−550 nm.

Fourier Transform Infrared Spectroscopy (FT-IR)

FT-IR spectra of the NCs-DOX were recorded with a Nicolet 6700 spectrometer using KBr pellet method and all of the spectra were obtained at a resolution of 4 cm^{-1}

and with a total of 32 scans with a wave number range between 500 and 4000 cm^{-1}.

Circular Dichroism Spectra (CD)

The CD spectra were recorded on a Chirascan CD spectrophotometer (Applied Photophysics, UK). CD spectra were determined over the range of 350−650 nm using a quartz cell with 0.1 mm path length. Scans were taken at a rate of 30 nm/min with a sampling interval of 1.0 nm and response time of 1 s at room temperature.

The Diameter and Size Distribution of Samples

The diameter and size distribution of the obtained NCs were evaluated by dynamic light scattering (DLS, Malvern Nano-ZS, UK) at sample concentration 1.0 mg/mL.

Staining of the NCs and NCs-DOX Structures by PTA for TEM Analysis

Generally, 3 μL of various NCs (1 mg/mL) was loaded on a carbon-coated TEM grid for 30 s and then dried using filter paper. A droplet of 5 μL of 2% PTA aqueous solution was then loaded on the sample containing the TEM grid to achieve different staining effects and dried using filter paper.

Cell Culture

RAW264.7 cell and MCF-7 cell were cultured in Dulbecco's Modified Eagle's Medium (DMEM) supplemented with 10% fetal bovine serum, 100 IU/mL penicillin, and 100 μg/mL streptomycin at 37 °C in a humidified atmosphere with 5% CO_2.

Cellular Uptake

The cellular uptake of NCs-DOX and free DOX were measured by fluorescence image. Briefly, MCF-7 cells at logarithm phase were seeded in 24 well cell culture plates at a cell density of 2×10^4 cells/well, respectively. After incubated for 24 h, NCs-DOX or free DOX dissolved in PBS at 5 mg/L was added to replace the media in each well. After further incubated for 4, and 12 h, the media were removed and these wells were rinsed with PBS (pH = 7.4). The cell nuclei were then stained with DAPI and were observed using a Nikon microscope (TE2000-U, Nikon, Japan). DOX was excited at 485 nm with the emission at 595 nm.[50]

MTT Assays

The therapeutic effect of NCs-DOX in vitro against the MCF-7 breast cells were incubated with free DOX and NCs-DOX for 24 hours and 48 hours, and the cell viability was measured by using a standard 3-(4,5-dimethyl-2-thia-zolyl)-2,5-diphenyl-2-H-tetrazolium bromide (MTT) assay.[51] Briefly, MCF-7 cells were cultured in 96-well plates at a density of 4×10^3 cells/well overnight to allow the cells to adhere onto the culture plate surface. Then, 100 μL of the culture media, in which the equivalent DOX concentrations were 0.125, 0.25, 0.5, 1.0, 5.0, and 10.0 ug/mL, respectively, were used to substitute the media in each well. Cells were subsequently incubated for 1 day and then evaluated by MTT assay. Untreated control cells were regarded as 100% viable and all values were expressed as a percentage of the control.

Results and Discussion
Chemical and Chiral Fingerprints of YSG Derived NCs

Figure 1A shows the chemical structure and chain conformation of YSG. The chemical nature of the polysaccharides was verified by ^1H NMR. As shown in Figure 1B, the chemical shifts of pristine YSG are consistent with the previous studies.[47,52] The spectrum of depolymerized YSG is highly similar to the pristine one, indicating that the depolymerization process did not damage the glucosidic units. For the spectra of BG, the multiple sharp and strong peaks in the range of 0.8–2.3 ppm can be attributed to the protons of the newly grafted butyryl groups. The peaks in the range of 3.0–5.5 ppm, where the proton signals on the β-glucan backbones are dominant, weakened significantly after chemical modification, indicating a high degree of substitution (DS) of butyryl groups for BG. The DS of BG was further determined to be 2.6 by titration techniques.

The chiral fingerprints of the NCs were then characterized by induced circular dichroism (ICD). β-glucans can exist in architectures with different chiral characteristics in solution, but they cannot be directly examined by CD owing to the lack of chromogenic groups. Congo red (CR) can probe the chirality of the assemblies of β-glucans in solution.[48,53] Although CR and β-glucans which have no CD signals, the chiral interaction of CR and helical motifs of β-glucan can lead to induced CD signals, and they are the chiral fingerprints of β-glucan nanostructures. As shown in Figure 1C, unesterified β-glucan NCs, including YG, GG, and SSG, show the strongest ICD bands at ~520 nm (Band-C) near the max UV-Vis
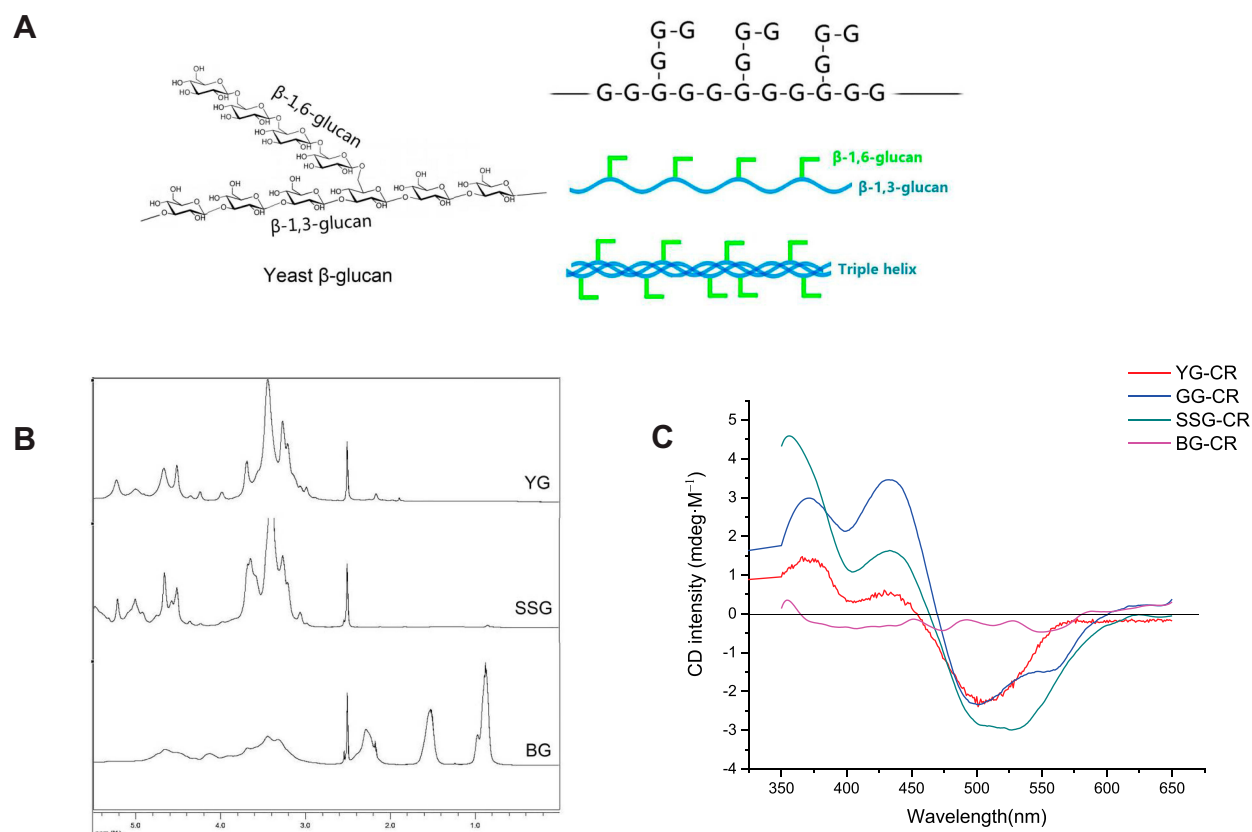
Figure I Chemical structure and chain conformations of YSG (**A**). ^{1}H NMR spectra of YG, SSG, and BG in d-DMSO (**B**). ICD spectra of YG, GG, SSG, and BG, complexed with Congo red (**C**).

absorption band of CR, which indicates that helical motifs are dominant in these NCs. In addition, all of the three unesterified carriers show twin positive bands at ~380 nm (Band-A) and ~440 nm (Band-B), respectively. However, the relative intensity of Band-A to Band-B is different. The ratio Band-A/Band-B is the highest for SSG, which is followed by YG and GG. The subtle difference in ICD spectra indicates a different chiral nanostructure of the NCs, and may affect the drug loading ability and immunological activity. In contrast, BG-CR only shows particularly weak ICD signal from 350 nm to 650 nm, and the band at ~520 nm is nearly undetectable, indicating that chains of BG exist in random coil state.

The Immune-Potentiation Properties of β-Glucan NCs Evaluated by a RAW264.7 Cell Model

β-glucans have been used as anti-tumor adjuvants based on their immunostimulatory activities such as activation of macrophage/dendritic cells, but such property is strongly affected by the state of molecular aggregation and secondary structures. Therefore, whether YG, GG, SSG, BG NCs activate RAW264.7 cells were examined by analysis of the mRNA expression of IL-1β, IL-6, TNF-α, IFN-γ. The expression levels of IL-1β, IL-6, TNF-α, IFN-γ in NCs-treated (400ug/mL) RAW264.7 cells were examined by RT-PCR after 24 h of incubation. As shown in Figure 2, the chiral negative ones such as BG do not stimulate RAW264.7 cells whereas chiral positive ones, such as YG, GG and SSG can activate RAW264.7 cells. However, there is also subtle difference in the activation effects for the 4 types of cytokines.

This subtle difference can induce the increase of expression of IL-1β mRNA by 5.64-fold, the IL-6 mRNA by 193.89-fold and the TNF-α mRNA by 3.90-fold, respectively, for YG NCs. For GG NCs, it can induce the increase of expression of the IL-1β mRNA by 22.72-fold, the IL-6 mRNA by 27.62-fold, the TNF-α mRNA by 1.89-fold and the IFN-γ mRNA by 13.73-fold, respectively. For SSG
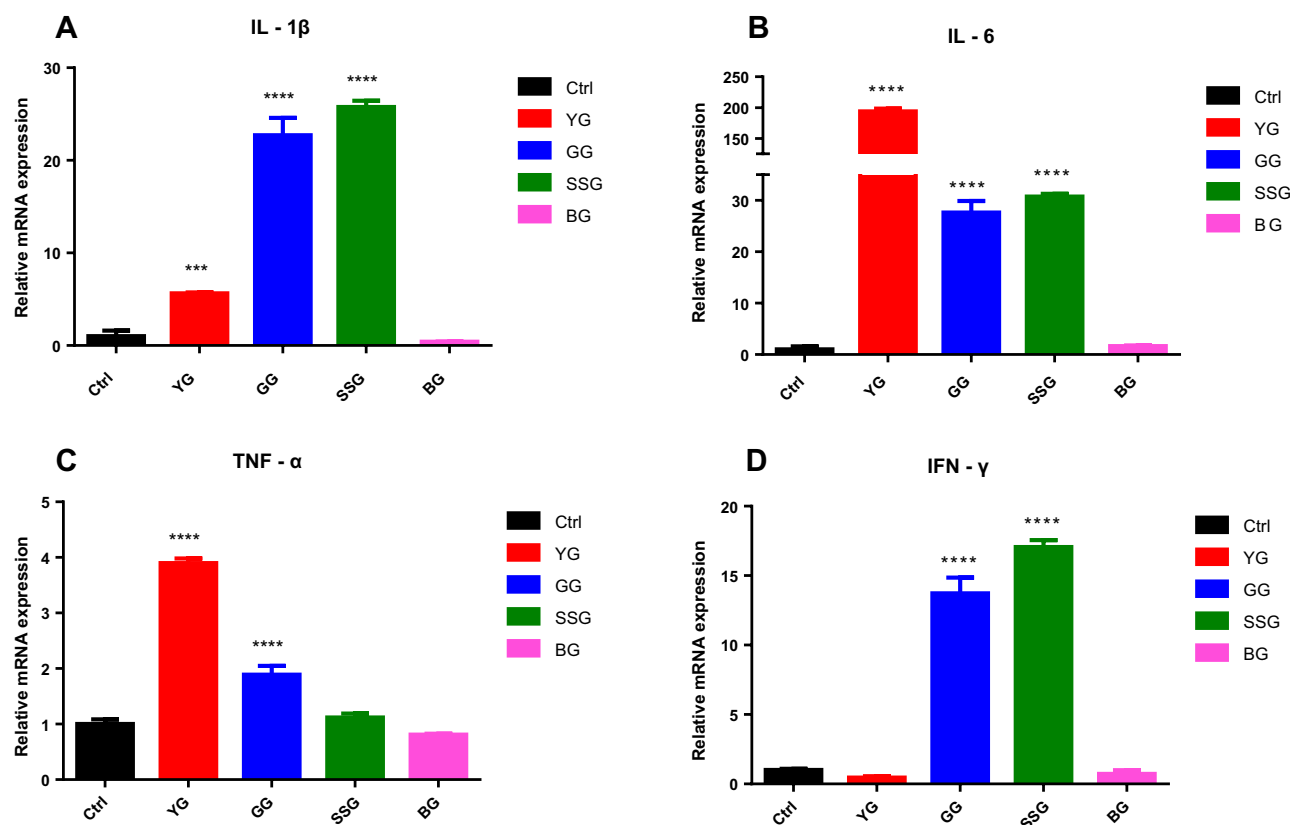
Figure 2 Effects of YG, GG, SSG, BG NCs on the expression of IL-1β, IL-6, TNF-α, IFN-γ in RAW264.7 macrophages. Cells were cultured in the presence of NCs (400 μg/mL) for 24 h and the expression of IL-1β (**A**), IL-6 (**B**), TNF-α (**C**), IFN-γ (**D**) mRNAs was measured using RT-PCR. Relative increases in the levels of each band compared with the loading control β-actin. Values are expressed as the mean ± SEM of the three separate experiments. Each group compared with the NCs-untreated cells (0 μg/mL). ***$p < 0.001$, ****$p < 0.0001$.

NCs, it can induce the increase of expression of the IL-1β mRNA by 25.76-fold, the IL-6 mRNA by 30.73-fold, the TNF-α mRNA by 1.12-fold and the IFN-γ mRNA by 17.05-fold, respectively.

In summary, β-glucan can maintain the immunostimulatory activity when the chirality was maintained, and the subtle difference in chiral fingerprints may induce a different gene expression profile of cytokines. There is evidence that the state of aggregation of β-glucan may affect its induction of different set of cytokines; however, the exact structural-property relationship is still not very clear.[54]

The DOX Encapsulation Ability of NCs

Figure 3A shows the photographs of YG, GG, SSG, and BG NCs after DOX was encapsulated. The suspensions are highly homogenous and can remain stable for at least 2 months. As shown in Table 1, the drug encapsulation efficiency of SSG-DOX, GG-DOX, YG-DOX and BG-DOX is 38.2%, 35.6%, 13.9% and 15.2%, respectively. This indicates that chiral fingerprints of NCs with such as

a higher ICD Band-A/Band-B ratio are associated with a higher drug encapsulation efficiency.

DLS was used to measure the particle size and distribution of the drug-loaded NCs. As shown in Figure 3B, the size distribution of these DOX-loaded NCs ranges from 50 nm to 160 nm. GG-DOX has the smallest average diameter around 50 nm. BG-DOX showed the largest average diameter of ~150 nm. YG-DOX and SSG-DOX have a particle size around 100 nm.

TEM examination is used to analyze the morphology of DOX-loaded NCs. As shown in Figure 3C, YG-DOX has a gel like morphology and fibrous network can be observed inside. The fibrous network can be attributed to the bundles of β-glucan triple helices, which have been observed in previous studies.[48] DOX may be entrapped in the water phase of the nano-sized gel. In contrast, GG-DOX exhibits a rectangular shape and a higher magnification image shows a lattice-like structure inside of the particles. We speculate that GG and DOX may have certain specific interaction, which leads to a formation of
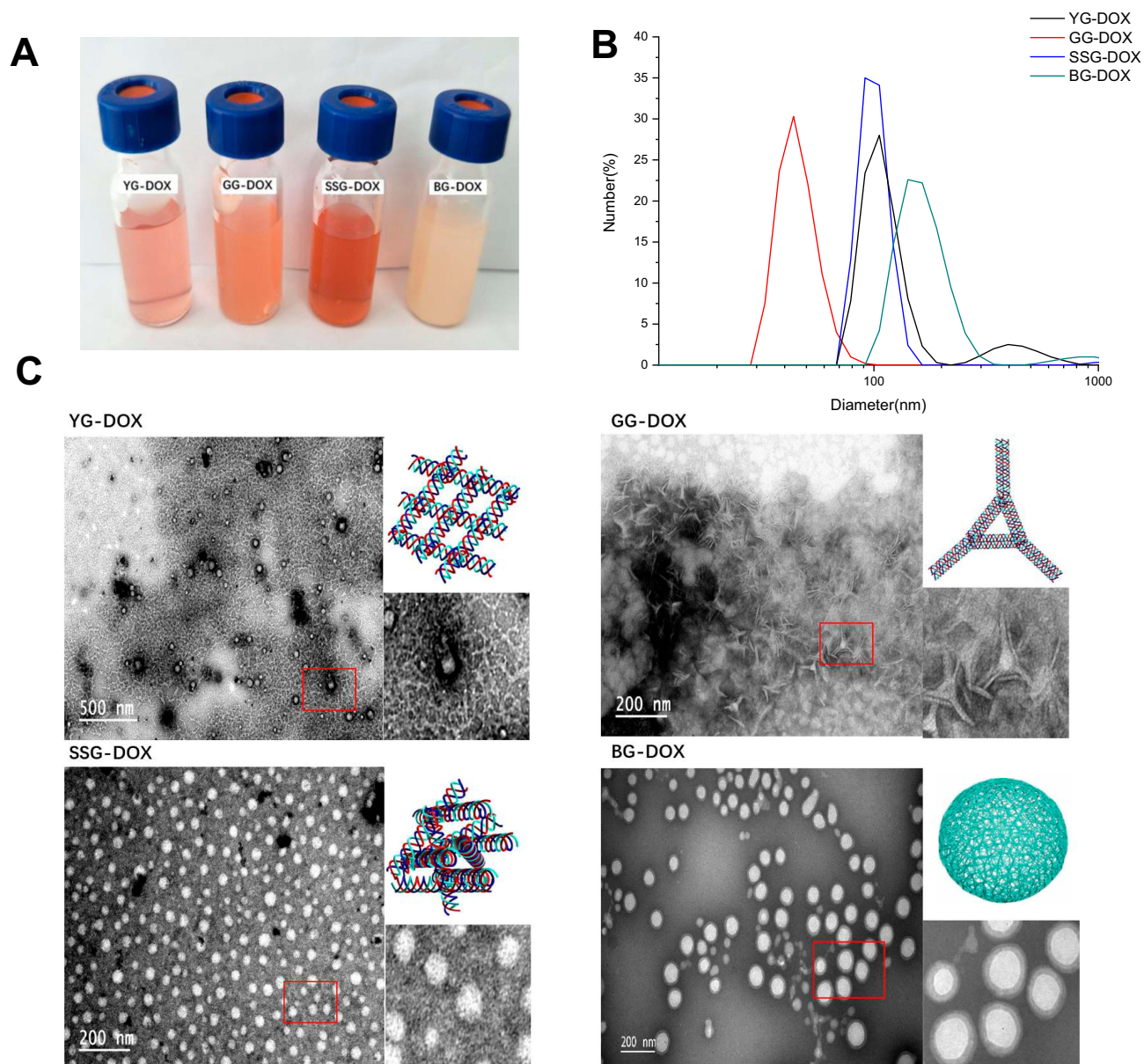
Figure 3 Photographs of the suspensions of DOX loaded NCs (**A**). Particle size and distributions of DOX loaded NCs measured by DLS (**B**). TEM images of the DOX loaded NCs (**C**).

highly organized assemblies. As for SSG-DOX and BG-DOX, spherical nanoparticles can be observed, but SSG-DOX seems to be less dense than BG-DOX. Hydrophobic

Table 1 Drug Encapsulation Efficiency (Wt%) of NCs-DOX

DOX	0.5	1	1.5	2
YG-DOX	10.5	11.9	13.5	12.6
GG-DOX	26.8	35.6	35.3	36.5
SSG-DOX	29.0	38.2	39.3	36.4
BG-DOX	13.3	15.2	14.1	17.2

Abbreviations: wt%, weight percent; NCs, nanocarriers; DOX, doxorubicin.

interaction may promote butyrylated β-glucan to aggregate more densely in water.

Chiral Interaction of β-Glucan NCs and DOX Studied by CD, UV-Vis, and FT-IR Spectroscopy

As DOX and β-glucan are both chiral molecules, possible chiral interactions were studied by CD spectra to reveal the drug loading mechanism of β-glucan NCs. DOX is a chiral molecule, which shows a split-type CD spectrum with a positive band at ~450 nm and a negative band at ~530 nm near the max absorption of DOX in the visible

light region. As shown in Figure 4A, when DOX was loaded into different NCs, the CD bands of DOX changed greatly, which reflects that DOX was loaded in different mechanisms. Strikingly, the CD bands of DOX were completely reversed when it was loaded into SSG, in which the highest drug loading efficiency was achieved. The drastic change in CD signals of DOX when encapsulated indicates that SSG and DOX may have highly specific chiral interactions. Also, when it was loaded in GG, the 530 nm band of DOX showed a significant upper-shift from negative zone to positive zone, indicating another type of chiral interaction of GG and DOX. However, the CD bands of DOX were nearly unchanged when loaded in YG, which shows a gel-like structure, indicating that the interaction is likely to be a non-specific physical absorption. The CD signals of DOX are largely shielded when loaded in BG, which may be caused by the high opacity of hydrophobic nanoparticles in water suspension. In summary, the drug encapsulation mechanisms of SSG and GG are based on chiral interactions between DOX and β-glucan helical moieties.

UV-Vis spectra were performed to analyze the DOX loading mechanism of NCs further. As shown in Figure 4B, both GG-DOX and SSG-DOX are capable of inducing a red shift of λ_{max} of DOX from 481 to 486 nm and from 481 to 492 nm, respectively, indicating that DOX may be encapsulated based on specific non-covalent interactions such as chiral interactions, rather than physical absorption. However, no obvious red shifts occur when DOX was loaded in YG, suggesting that DOX was entrapped by non-specific absorption. That shows no absorption peak for BG-DOX NCs from 450 to 550 nm and the peak of DOX may be shielded by high opacity of BG suspension.

FT-IR was used to verify the encapsulation of DOX in NCs. Figure 4C shows the FT-IR spectra of DOX, YSG, and NCs-DOX. For YSG, the absorption at ~3395 cm^{-1} (O-H stretching), ~2920 cm^{-1} (C-H stretching), ~1646 cm^{-1} (C-O stretching), ~1153 cm^{-1} (bridge-O stretching) and ~1077 cm^{-1} (secondary O-H stretching) can be attributed to β-glucan. For butyryl β-glucan, the new peak at ~1738 cm^{-1} corresponding to the C=O stretch vibration demonstrated the successful esterification. For DOX, the characteristic
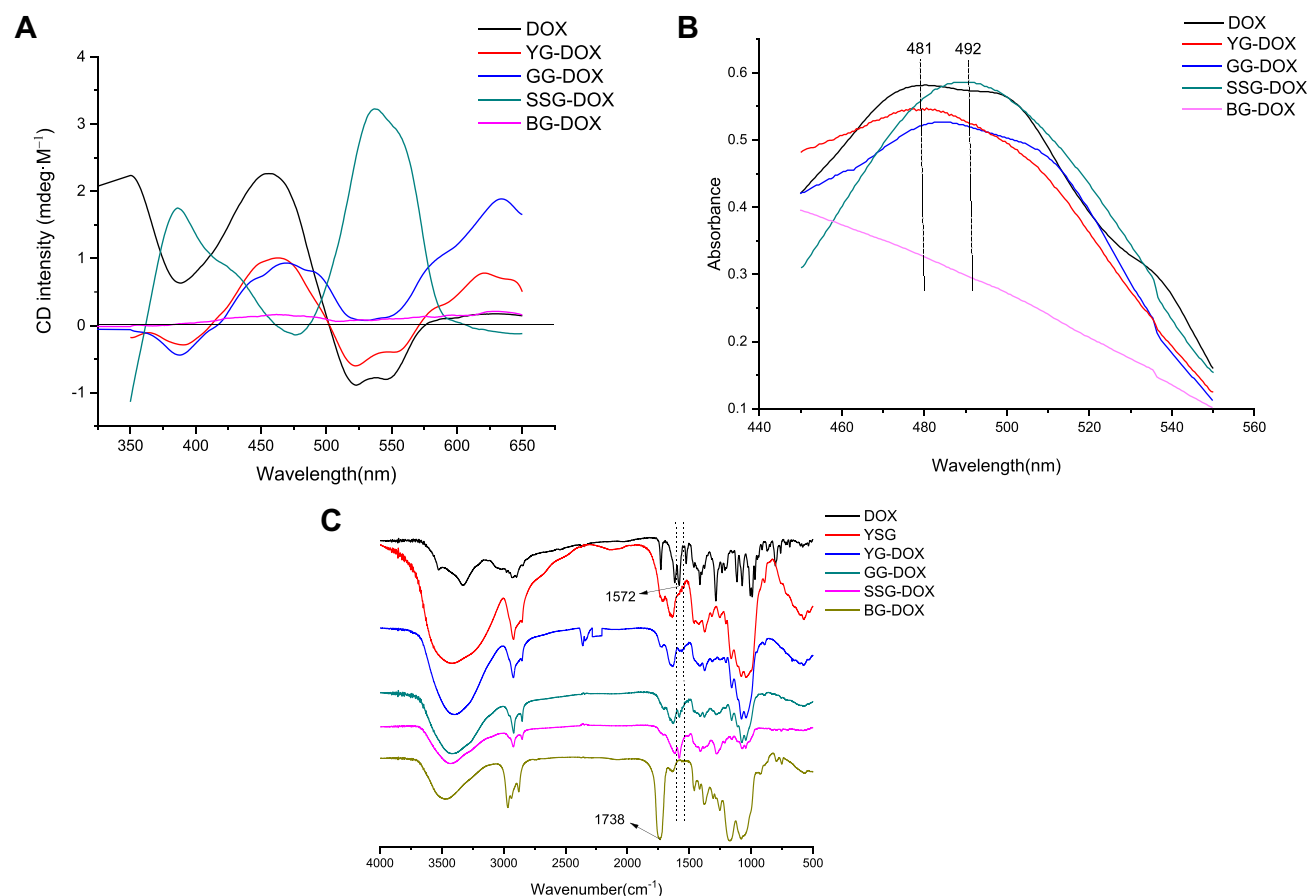
Figure 4 CD spectral analysis for the DOX loaded NCs (**A**). UV-Vis spectra for the DOX loaded NCs (**B**). FT-IR spectra for the DOX loaded NCs (**C**).

absorption peak at ~1572 cm^{-1} assigned to the stretching band of the aromatic rings of DOX. Compared with the free DOX and NCs, the appearance of typical bands at ~1572 cm^{-1} in DOX-loaded nanoparticles was a proof that DOX was successfully loaded in YG, GG, SSG and BG NCs. Moreover, the higher absorbance of ~1572 cm^{-1} indicated that GG and SSG have better DOX loading capacity.

The Drug Release Profile of the NCs-DOX

The drug release profile of the NCs-DOX were evaluated under normal physiological conditions (pH = 7.4) and under tumor microenvironment where the pH value is lower than the normal tissue (pH = 5.0). The drug release behavior of the above four nanoparticles was determined by a dialysis method in PBS of pH = 7.4 and pH = 5.0. The results (Figure 5) show that 30%, 26% and 24% of the loaded DOX was released from BG-DOX, SSG-DOX and GG-DOX within 12 h at pH = 5.0, respectively. However, only 18% of the loaded DOX was released from YG-DOX. The cumulative release of DOX in the buffer of pH = 5.0 revealed a sustained release over the entire period of study. For BG-DOX, the cumulative release reaches a plateau with 41% of DOX and the YG-DOX, GG-DOX, SSG-DOX were 20%, 36%, 38% of DOX, respectively. Thus, the higher release rate of SSG-DOX and GG-DOX over YG-DOX may indicate that the chiral interactions between DOX and NCs can be affected by pH change of microenvironment, resulting in a pH-sensitive DOX release.

## Cellular Uptake and Cytotoxicity

Fluorescence microscopy was used to study the cellular uptake of free DOX and NCs-DOX. DOX kills tumor cell by intercalating DNA and RNA in the nuclei. In addition, free DOX diffuses into nuclei because of their high affinity with nucleic acids, but normal nanoparticles that are internalized through endocytosis pathway generally entrap the DOX in endosome/lysosome. Figure 6A illustrates the observation on cellular uptakes of free DOX and NCs-DOX into MCF-7 after 4 h and 12 h. For free DOX and YG-DOX, GG-DOX, SSG-DOX, it can be observed that red fluorescence concentrated around the nucleus area after 4 h and entered into the nucleus after 12 h, indicating that YG-DOX, GG-DOX, SSG-DOX NCs can successfully deliver DOX to the nuclear region to kill cancer cells.

As for BG-DOX, the cells exhibited strongest red fluorescence after treatment with the BG-DOX NCs compared with the free DOX and other NCs-DOX both after 4 h and 12 h. However, BG-DOX shows severe aggregation in the medium. Excessive hydrophobic groups in BG may cause the absorption of proteins and cause deformation of cell membrane. The red fluorescence of BG-DOX was uneven distribution and few in the area of nucleus suggesting that BG-DOX NCs are not efficient to deliver drugs to the nuclear region successfully. In summary, GG and SSG NCs effectively deliver DOX into the cell and into the nucleus. However, BG is not conducive to drug delivery may cause by its excessive presence of hydrophobic groups.
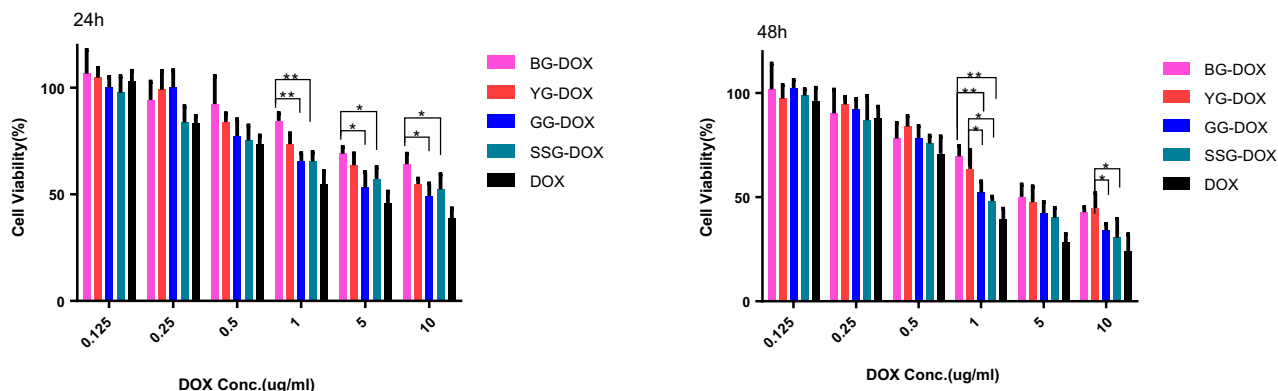
MTT cell proliferation assay was employed to measure the cellular toxicity of free DOX and NCs-DOX (Figure 6B). For the analysis of antiproliferative activities at 24 h and 48
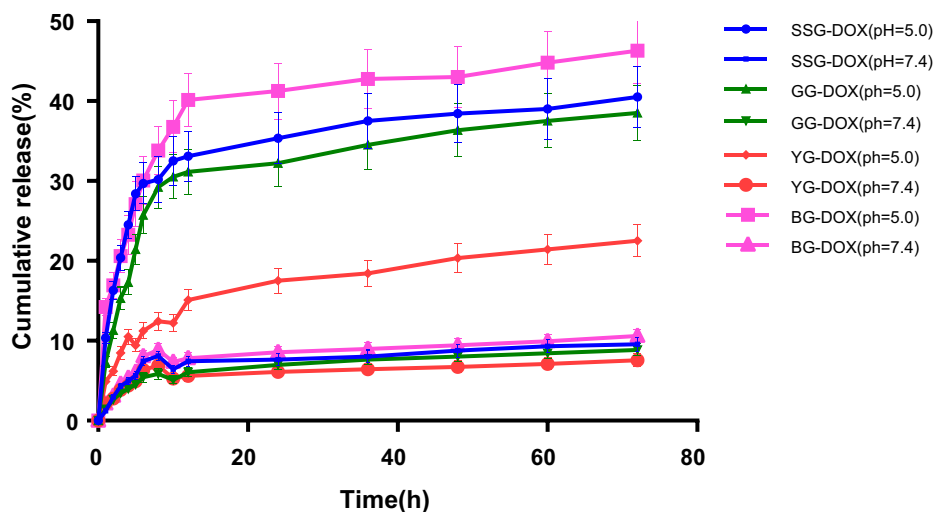
Figure 5 In vitro release profiles of DOX from NCs at pH = 5.0 and pH = 7.4 within 72 h.

A
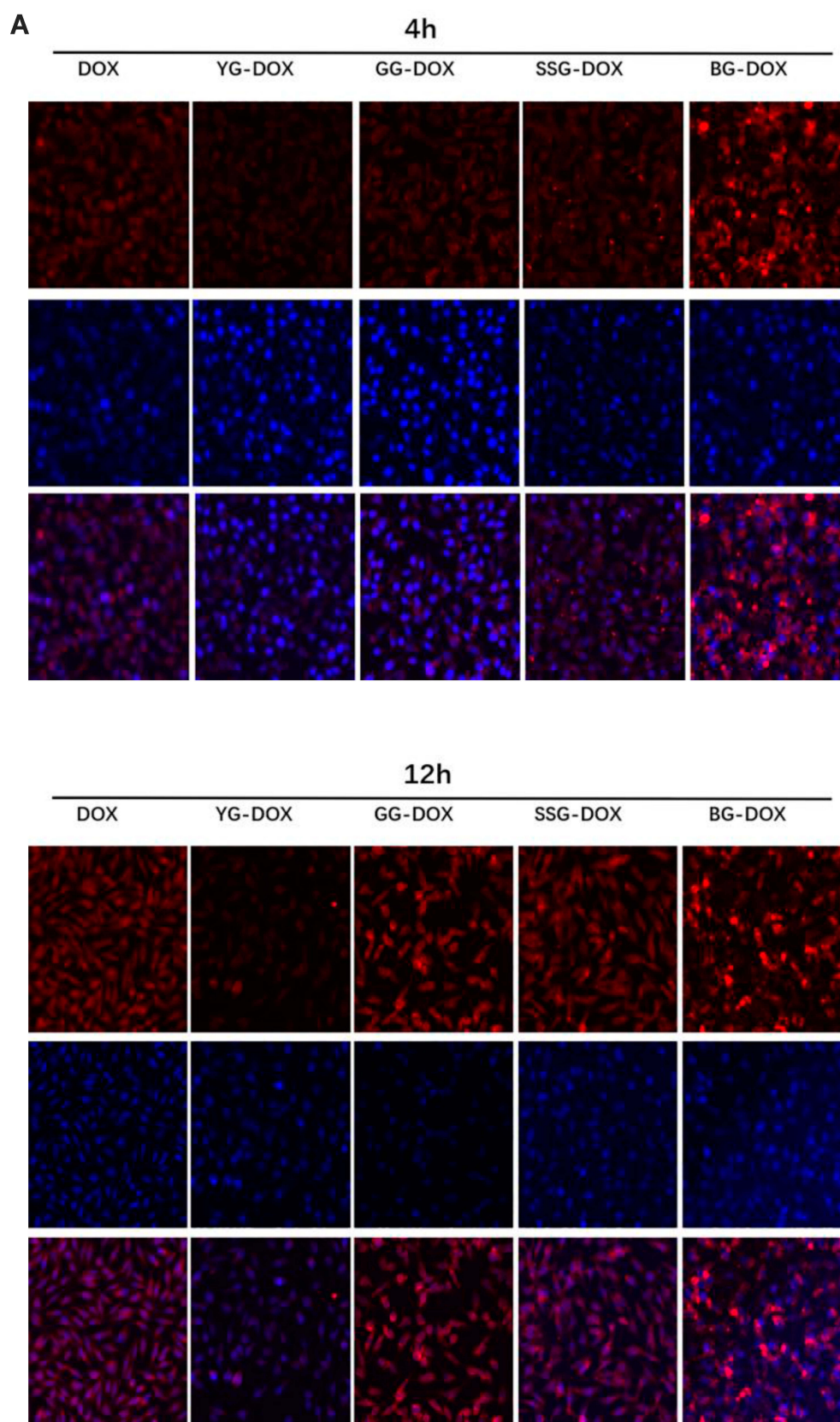
Figure 6 Continued.

B

Figure 6 Fluorescence microscopic images of MCF-7 cells treated with DOX loaded NCs and free DOX for 4 h and 12 h (**A**). Cytotoxicity of DOX loaded NCs and free DOX against MCF-7 cells for 24 h and 48 h (**B**). *p < 0.05, **p < 0.01.

h, NCs-DOX and free DOX against MCF-7 cells were gradually improved with time and the increased concentration of DOX. After incubation of 24 h, the half-maximal inhibitory concentration (IC_{50}) value (Table 2) of DOX (3.328 μg/mL) was extremely smaller than that of YG-DOX (11.74 μg/mL), GG-DOX (6.736 μg/mL), SSG-DOX (9.213 μg/mL) and BG-DOX (20.13 ug/mL) suggesting that the free DOX exerted stronger cytotoxicity compared with NCs-DOX. This might be attributed to the fact that the free DOX with low molecular weight could be internalized rapidly via diffusion approach and displayed antiproliferative function through inhibiting nucleic acid synthesis. As for the NCs-DOX, it had to release DOX under the acid microenvironment before exhibiting cytotoxicity, which was in keeping with the analysis of cellular uptake results.

Conclusion

A series of chiral nanoparticles based on polysaccharides β-glucan were prepared by simple denaturation-renaturation approaches and their nanostructures and chiral properties were characterized by various spectroscopy and microscopy techniques. The incorporation of anti-cancer drug

Table 2 IC_{50}(Ug/Ml) of DOX and NCs-DOX for MCF-7 Cell

IC_{50}(ug/mL)	24h	48h
DOX	3.328	1.331
YG-DOX	11.74	5.087
GG-DOX	6.736	2.862
SSG-DOX	9.213	2.274
BG-DOX	20.13	5.244

Abbreviations: NCs, nanocarriers; DOX, doxorubicin; MCF-7, human breast cancer cell.

DOX into these nanoparticles induced drastic changes in the CD spectra of DOX, indicating a special chiral interaction between the carrier and the drug. In addition, these chiral active nanoparticles also show strong immunopotentiation ability and high drug loading efficiency. These nanoparticles can be developed as a novel type of nanomedicine for anti-cancer treatment.

Disclosure

The authors report no conflicts of interest in this work.

References

1. Swierczewska M, Han HS, Kim K, et al. Polysaccharide-based nanoparticles for theranostic nanomedicine. *Adv Drug Deliv Rev.* 2016;99:70–84. doi:10.1016/j.addr.2015.11.015

2. Mohammadi G, Zangeneh MM, Zangeneh A, et al. Chemical characterization and anti-breast cancer effects of silver nanoparticles using Phoenix dactylifera seed ethanolic extract on 7,12-dimethylbenz[a] anthracene-induced mammary gland carcinogenesis in sprague dawley male rats. *Appl Organomet Chem*. 2020;34(1):e5136. doi:10.1002/aoc.5136

3. Shahriari M, Hemmati S, Zangeneh A, et al. Biosynthesis of gold nanoparticles using Allium noeanum reut. ex regel leaves aqueous extract; characterization and analysis of their cytotoxicity, antioxidant, and antibacterial properties. *Appl Organomet Chem*. 2019;33(11):e5189. doi:10.1002/aoc.5189

4. Hoshyar N, Gray S, Han H, et al. The effect of nanoparticle size on in vivo pharmacokinetics and cellular interaction. *Nanomedicine.* 2016;11(6):673–692. doi:10.2217/nnm.16.5

5. Hemmati S, Zamenian T, Delsooz N, et al. Preparation and synthesis a new chemotherapeutic drug of silver nanoparticle-chitosan composite; chemical characterization and analysis of their antioxidant, cytotoxicity, and anti-acute myeloid leukemia effects in comparison to daunorubicin in a leukemic mouse model. *Appl Organomet Chem.* 2020;34:e5274. doi:10.1002/aoc.5274

6. Ahmeda A, Zangeneh A, Zangeneh MM. Preparation, formulation, and chemical characterization of silver nanoparticles using Melissa officinalis leaf aqueous extract for the treatment of acute myeloid leukemia in vitro and in vivo conditions. *Appl Organomet Chem.* 2020;34:e5378. doi:10.1002/aoc.5378

7. Goorani S, Koohi MK, Morovvati H, et al. Application of natural compounds–based gold nanoparticles for the treatment of hemolytic anemia in an anemic mouse model: formulation of a novel drug from relationship between the nanotechnology and hematology sciences. *Appl Organomet Chem*. 2020;34(4):e5475. doi:10.1002/aoc.5475

8. Zangeneh MM, Zangeneh A, Pirabbasi E, et al. Falcaria vulgaris leaf aqueous extract mediated synthesis of iron nanoparticles and their therapeutic potentials under in vitro and in vivo condition. *Appl Organomet Chem.* 2019;33(12):e5246. doi:10.1002/aoc.5246

9. Zhaleh M, Zangeneh A, Goorani S, et al. In vitro and in vivo evaluation of cytotoxicity, antioxidant, antibacterial, antifungal, and cutaneous wound healing properties of gold nanoparticles produced via a green chemistry synthesis using Gundelia tournefortii L. as a capping and reducing agent. *Appl Organomet Chem*. 2019;33:e5015. doi:10.1002/aoc.5015

10. Shahriari M, Hemmati S, Zangeneh A, et al. Decoration of silver nanoparticles on multi-walled carbon nanotubes: investigation of its anti-acute leukemia property against acute myeloid leukemia and acute T cell leukemia. *Appl Organomet Chem*. 2020;34(4). doi:10.1002/aoc.5476.

11. Ma L, Ahmeda A, Wang K, et al. Introducing a novel chemotherapeutic drug formulated by iron nanoparticles for the clinical trial studies. *Appl Organomet Chem*. 2020. doi:10.1002/aoc.5498

12. Tahvilian R, Zangeneh MM, Falahi H, et al. Green synthesis and chemical characterization of copper nanoparticles using Allium saralicum leaves and assessment of their cytotoxicity, antioxidant, antimicrobial, and cutaneous wound healing properties. *Appl Organomet Chem*. 2019;33(12):e5234. doi:10.1002/aoc.5234

13. Seydi N, Saneei S, Jalalvand AR, et al. Synthesis of titanium nanoparticles using Allium eriophyllum boiss aqueous extract by green synthesis method and evaluation of their remedial properties. *Appl Organomet Chem*. 2019;33(11):e5191. doi:10.1002/aoc.5191

14. Mahdavi B, Saneei S, Qorbani M, et al. Ziziphora clinopodioides lam leaves aqueous extract mediated synthesis of zinc nanoparticles and their antibacterial, antifungal, cytotoxicity, antioxidant, and cutaneous wound healing properties under in vitro and in vivo conditions. *Appl Organomet Chem*. 2019;33(11):e5164. doi:10.1002/aoc.5164

15. Zangeneh MM. Green synthesis and chemical characterization of silver nanoparticles from aqueous extract of Falcaria vulgaris leaves and assessment of their cytotoxicity and antioxidant, antibacterial, antifungal and cutaneous wound healing properties. *Appl Organomet Chem*. 2019;33(9):e4963.

16. Zangeneh MM, Bovandi S, Gharehyakheh S, et al. Green synthesis and chemical characterization of silver nanoparticles obtained using Allium saralicum aqueous extract and survey of in vitro antioxidant, cytotoxic, antibacterial and antifungal properties. *Appl Organomet Chem*. 2019;33:e4961. doi:10.1002/aoc.4961

17. Seydi N, Mahdavi B, Paydarfard S, et al. Preparation, characterization, and assessment of cytotoxicity, antioxidant, antibacterial, antifungal, and cutaneous wound healing properties of titanium nanoparticles using aqueous extract of Ziziphora clinopodioides lam leaves. *Appl Organomet Chem*. 2019;33:e5009. doi:10.1002/aoc.5009

18. Zangeneh MM, Saneei S, Zangeneh A, et al. Preparation, characterization, and evaluation of cytotoxicity, antioxidant, cutaneous wound healing, antibacterial, and antifungal effects of gold nanoparticles using the aqueous extract of Falcaria vulgaris leaves. *Appl Organomet Chem*. 2019;33(11):e5216. doi:10.1002/aoc.5216

19. Mahdavi B, Paydarfard S, Zangeneh MM, et al. Assessment of antioxidant, cytotoxicity, antibacterial, antifungal, and cutaneous wound healing activities of green synthesized manganese nanoparticles using Ziziphora clinopodioides lam leaves under in vitro and in vivo condition. *Appl Organomet Chem*. 2020;34(1):e5248. doi:10.1002/aoc.5248

20. Hamelian M, Zangeneh MM, Shahmohammadi A, et al. Pistacia atlantica leaf extract mediated synthesis of silver nanoparticles and their antioxidant, cytotoxicity, and antibacterial effects under in vitro condition. *Appl Organomet Chem*. 2020;34(1):e5278. doi:10.1002/aoc.5278

21. Hemmati S, Rashtiani A, Zangeneh MM, et al. Green synthesis and characterization of silver nanoparticles using fritillaria flower extract and their antibacterial activity against some human pathogens. *Polyhedron*. 2018.

22. Zangeneh MM, Joshani Z, Zangeneh A, et al. Green synthesis of silver nanoparticles using aqueous extract of Stachys lavandulifolia flower, and their cytotoxicity, antioxidant, antibacterial and cutaneous wound-healing properties. *Appl Organomet Chem*. 2019

23. Dacoba TG, Omange RW, Li H, et al. Polysaccharide nanoparticles can efficiently modulate the immune response against an HIV peptide antigen. *ACS Nano*. 2019;13:4947–4959. doi:10.1021/acsnano.8b07662

24. Frauenfeld J, Löving R, Armache JP, et al. A saposin-lipoprotein nanoparticle system for membrane proteins. *Nat Methods*. 2016;13(4):345–351. doi:10.1038/nmeth.3801

25. Ball RL, Hajj KA, Vizelman J, et al. Lipid nanoparticle formulations for enhanced co-delivery of siRNA and mRNA. *Nano Lett*. 2018;18(6):3814–3822. doi:10.1021/acs.nanolett.8b01101

26. Buck J, Grossen P, Cullis PR. Lipid-based DNA therapeutics: hallmarks of non-viral gene delivery. *ACS Nano*. 2019;13:3754–3782. doi:10.1021/acsnano.8b07858

27. Ao Y, Zeng K, Yu B, et al. An upconversion nanoparticle enables near infrared-optogenetic manipulation of the caenorhabditis elegans motor circuit. *ACS Nano*. 2019;13:3373–3386. doi:10.1021/acsnano.8b09270

28. Zhang Y, Sun T, Jiang C. Biomacromolecules as carriers in drug delivery and tissue engineering. *Acta Pharm Sin B*. 2017;8(1):34–50. doi:10.1016/j.apsb.2017.11.005

29. Nitta SK, Numata K. Biopolymer-based nanoparticles for drug/gene delivery and tissue engineering. *Int J Mol Sci*. 2013;14(1):1629–1654. doi:10.3390/ijms14011629

30. Hong S, Zhang Z, Liu H, et al. B cells are the dominant antigen-presenting cells that activate naive CD4(+) T cells upon immunization with a virus-derived nanoparticle antigen. *Immunity*. 2018;49(4):695–708.e694. doi:10.1016/j.immuni.2018.08.012

31. Lu D, Zhou J, Hou S, et al. Functional macromolecule-enabled colloidal synthesis: from nanoparticle engineering to multifunctionality. *Adv Mater.* 2019;31:e1902733. doi:10.1002/adma.201902733

32. Liu Q, Duan B, Xu X, et al. Progress in rigid polysaccharide-based nanocomposites with therapeutic functions. *J Mater Chem B.* 2017;5 (29):5690–5713. doi:10.1039/c7tb01065f

33. Numata M, Shinkai S. 'Supramolecular wrapping chemistry' by helix-forming polysaccharides: a powerful strategy for generating diverse polymeric nano-architectures. *Chem Commun.* 2011;47 (7):1961–1975. doi:10.1039/C0CC03133J

34. Yashima E, Maeda K, Iida H, et al. Helical polymers: synthesis, structures, and functions. *Chem Rev.* 2009;109(11):6102–6211. doi:10.1021/cr900162q

35. Okamoto Y, Yashima E. Polysaccharide derivatives for chromatographic separation of enantiomers. *Angew Chem Int Ed Engl.* 1998;37(8):1020–1043. doi:10.1002/(sici)1521-3773(19980504) 37:8<020::aid-anie1020><020::aid-anie1020>3.0.co;2–5

36. Duan B, Li M, Sun Y, et al. Orally delivered antisense oligodeoxyribonucleotides of TNF-α via polysaccharide-based nanocomposites targeting intestinal inflammation. *Adv Healthc Mater.* 2019;8 (5):1801389. doi:10.1002/adhm.201801389

37. Liu Q, Wang C, Cao Y, et al. A novel gene carrier prepared from triple helical β-glucan and polydeoxyadenylic acid. *J Mater Chem B.* 2014;2(8):933–944. doi:10.1039/C3TB21195A

38. Shiraki T, Dawn A, Tsuchiya Y, et al. Thermo- and solvent-responsive polymer complex created from supramolecular complexation between a helix-forming polysaccharide and a cationic polythiophene. *J Am Chem Soc.* 2010;132(39):13928–13935. doi:10.1021/ja1067349

39. Zhong D, Jiao Y, Zhang Y, et al. Effects of the gene carrier polyethyleneimines on structure and function of blood components. *Biomaterials.* 2013;34(1):294–305. doi:10.1016/j.biomaterials.2012.09.060

40. Adams D, Nathans R, Pero S, et al. Activation of a rel-A/CEBP-beta-related transcription factor heteromer by PGG-glucan in a murine monocytic cell line. *J Cell Biochem.* 2000;77(2):221–233. doi:10.1002/(SICI)1097-4644(20000501)77:2<221::aid-jcb6>3.0. CO;2–V

41. Lee K, Kwon Y, Hwang J, et al. Synthesis and functionalization of β-glucan particles for the effective delivery of doxorubicin molecules. *ACS Omega.* 2019;4(1):668–674. doi:10.1021/acsomega.8b02712

42. Zhou J-L, Song F, Tian J-F, et al. Electrostatic wrapping of doxorubicin with curdlan to construct an efficient pH-responsive drug delivery system. *Nanotechnology.* 2017;28(29):295601. doi:10.1088/ 1361-6528/aa75b5

43. Meng Y, Zou S, Jiang M, et al. Dendritic nanotubes self-assembled from stiff polysaccharides as drug and probe carriers. *J Mater Chem B.* 2017;5(14):2616–2624. doi:10.1039/c7tb00213k

44. Zhang R, Edgar KJ. Properties, chemistry, and applications of the bioactive polysaccharide curdlan. *Biomacromolecules.* 2014;15 (4):1079–1096. doi:10.1021/bm500038g

45. Yanaki T, Norisuye T, Fujita H. Triple helix of schizophyllum commune polysaccharide in dilute solution. 3. hydrodynamic properties in water. *Macromolecules.* 1980;13(6):1462–1466. doi:10.1021/ ma60078a019

46. Berner VK, duPre SA, Redelman D, et al. Microparticulate β-glucan vaccine conjugates phagocytized by dendritic cells activate both naïve CD4 and CD8 T cells in vitro. *Cell Immunol.* 2015;298(1– 2):104–114. doi:10.1016/j.cellimm.2015.10.007

47. Wu C, Chu B, Kuang L, et al. Synthesis of β-1,3-glucan esters showing nanosphere formation. *Carbohydr Polym.* 2013;98(1):807– 812. doi:10.1016/j.carbpol.2013.06.056

48. Wu C, Huang J, Chu B, et al. Dynamic and hierarchically structured networks with tissue-like mechanical behavior. *ACS Nano.* 2019;13 (9):10727–10736. doi:10.1021/acsnano.9b05436

49. Mishra V, Jung SH, Park JM, et al. Triazole-containing hydrogels for time-dependent sustained drug release. *Macromol Rapid Commun.* 2014;35(4):442–446. doi:10.1002/marc.201300585

50. Li H, Cui Y, Sui J, et al. Efficient delivery of DOX to nuclei of hepatic carcinoma cells in the subcutaneous tumor model using pH-sensitive pullulan-DOX conjugates. *ACS Appl Mater Interfaces.* 2015;7(29):15855–15865. doi:10.1021/acsami.5b03150

51. Hansen MB, Nielsen SE, Berg K. Re-examination and further development of a precise and rapid dye method for measuring cell growth/ cell kill. *J Immunol Methods.* 1989;119(2):203–210. doi:10.1016/ 0022-1759(89)90397-9

52. Ensley HE, Tobias B, Pretus HA, et al. NMR spectral analysis of a water-insoluble (1 → 3)-β-d-glucan isolated from Saccharomyces cerevisiae. *Carbohydr Res.* 1994;258:307–311. doi:10.1016/0008- 6215(94)84098-9

53. Ogawa K, Hatano M. Circular dichroism of the complex of a (1→3)- β-d-glucan with congo red. *Carbohydr Res.* 1978;67(2):527–535. doi:10.1016/S0008-6215(00)84144-0

54. Goodridge HS, Reyes CN, Becker CA, et al. Activation of the innate immune receptor dectin-1 upon formation of a 'phagocytic synapse'. *Nature.* 2011;472(7344):471–475. doi:10.1038/nature10071